

1 **Repressor activity of SqrR, a master regulator of persulfide-responsive genes, is**
2 **regulated by heme coordination**

3

4 Running head: SqrR is a heme binding protein

5

6 Corresponding author: Takayuki Shimizu, Graduate School of Arts and Sciences, The
7 University of Tokyo, 3-8-1 Komaba, Meguro-ku, Tokyo 153-8902, Japan, Tel.: +81-3-5454-
8 6627; Fax: +81-3-5454-6627; E-mail: ctshimizu@g.ecc.u-tokyo.ac.jp

9

10 Subject areas:

11 (3) regulation of gene expression

12 (2) environmental and stress responses

13

14 Material:

15 Black and white figures: 2

16 Color figures: 2

17 Tables: 2

18 Supplementary material: 1 pdf file

19

20 **Repressor activity of SqrR, a master regulator of persulfide-responsive genes, is**
21 **regulated by heme coordination**

22

23 Running head: SqrR is a heme binding protein

24

25 Takayuki Shimizu^{1,2,3} *, Yuuki Hayashi³, Munehito Arai^{3,4}, Shawn E. McGlynn², Tatsuru
26 Masuda³, Shinji Masuda^{1,2}

27

28 ¹Department of Life Science and Technology, Tokyo Institute of Technology, Kanagawa,
29 Japan

30 ²Earth-Life Science Institute, Tokyo Institute of Technology, Tokyo, Japan

31 ³Graduate School of Arts and Sciences, The University of Tokyo, Tokyo, Japan

32 ⁴Department of Physics, The University of Tokyo, Tokyo, Japan

33

34 *Corresponding author: ctshimizu@g.ecc.u-tokyo.ac.jp

35

36 **Abstract**

37 Reactive sulfur species (RSS) are involved in bioactive regulation via persulfidation of
38 proteins. However, how cells regulate RSS-based signaling and RSS metabolism is poorly
39 understood, despite the importance of universal regulation systems in biology. We
40 previously showed that the persulfide-responsive transcriptional factor SqrR acts as a
41 master regulator of sulfide-dependent photosynthesis in proteobacteria. Here, we
42 demonstrated that SqrR also binds heme at a near one-to-one ratio with a binding constant
43 similar to other heme binding proteins. Heme does not change the DNA binding pattern of
44 SqrR to the target gene promoter region; however, DNA binding affinity of SqrR is reduced
45 by the binding of heme, altering its regulatory activity. Circular dichroism spectroscopy
46 clearly showed secondary-structural changes of SqrR by the heme-binding. Incremental
47 change of the intracellular heme concentration is associated with small, but significant
48 reduction of the transcriptional repression by SqrR. Overall, these results indicate that SqrR
49 has an ability to bind heme to modulate its DNA binding activity, which may be important
50 for precise regulation of RSS metabolism *in vivo*.

51

52 **Keywords**

53 heme sensor, persulfide sensor, transcriptional regulation, *Rhodobacter capsulatus*, photosynthetic
54 bacteria

55

56 **Introduction**

57 Hydrogen sulfide is both a toxic gas and an important signaling molecule that is involved in
58 various cellular processes including the regulation of antibiotic resistance in bacteria
59 (Shatalin et al., 2011), senescence, seed germination, root hair growth, and abiotic stress
60 responses in plants (Chen et al., 2019; Li et al., 2018, 2016; Wei et al., 2017). Emerging
61 evidence suggests that reactive sulfur species (RSS) are the actual sulfide signaling species
62 for this bioactive regulation (Cuevasanta et al., 2015; Ida et al., 2014; Nishida et al., 2012;
63 Yadav et al., 2016). RSS are oxidized sulfur species such as cysteine persulfide (CysSSH)
64 and glutathione persulfide (GSSH), and RSS are endogenously generated either by i) direct
65 reaction between H₂S, an oxidant (such as O₂), and low-molecule-weight (LMW) thiols, ii)
66 between H₂S and LMW disulfides, or iii) enzymatically, *e.g.* by cystathionine γ -lyase (CSE),
67 cystathionine β -synthase (CBS), cysteinyl-tRNA synthetase (CARS) and sulfide/quinone
68 oxidoreductases (SQR) (Akaike et al., 2017; Birke et al., 2015; Chen et al., 2015; Dóka et al.,
69 2016; Ida et al., 2014; Libiad et al., 2014; Nishida et al., 2012; Ono et al., 2014; Shen et al.,
70 2016; Yadav et al., 2016). Cysteine, with its thiol containing side chain, is the substrate for
71 persulfidation (*S*-sulfuration), and persulfidated proteins have key roles in signaling and also
72 biosynthetic processes (Aroca et al., 2017; Dóka et al., 2016; Ida et al., 2014; Luebke et al.,
73 2014; Mustafa et al., 2009; Shimizu and Masuda, 2020)

74 One of the most studied persulfide sensors is CstR (CsoR-like sulfurtransferase
75 repressor) in *Staphylococcus aureus*. CstR responds to persulfide by forming an
76 intermolecular tetrasulfide bond, which results in a loss of DNA-binding affinity to target
77 promoters (Luebke et al., 2014). CstR is a member of the CsoR/RcnR family of
78 metalloregulatory proteins (Chang et al., 2014) and is also able to be modified by selenite
79 (SeO₃²⁻) or tellurite (TeO₃²⁻) to form a mixture of intersubunit disulfides and selenotrisulfides
80 or tellurotrisulfides, respectively (Luebke et al., 2014, 2013). The DNA binding affinity of
81 CstR is reduced by these modification *in vitro* (Luebke et al., 2013); although the
82 transcriptional level of CstR-regulated genes are not changed by addition of SeO₃²⁻ in
83 cultures (Luebke et al., 2014). Thus, it is assumed that CstR could react with various
84 metalloid and non-metal cofactors *in vitro*; however, the RSS is the predominantly
85 functioning signaling molecule *in vivo*. Probably, the additional metal modifications may
86 fine-tune the function of CstR depending on environmental conditions of this bacterial
87 growth, but *in vivo* evidence is needed to substantiate this hypothesis.

88 As an additional small molecule with regulatory consequences, heme is known to

89 modify the DNA-binding activity of transcription factors, such as HrtR, which responds to
90 heme and facilitates gene expression of the heme efflux transporter to avoid cell damage
91 induced by excessive intracellular heme (Sawai et al., 2012). Additionally, PpsR, which
92 regulates the expression of tetrapyrrole and photosynthesis-related genes, also binds to heme
93 and changes its DNA binding affinity to modulate the amount of tetrapyrrole and
94 photosynthesis-related gene products (Yin et al., 2012). This activity thereby provides control
95 to avoid excess free tetrapyrrole accumulation. PpsR is widely conserved among
96 photosynthetic bacteria and is well known redox sensor as it has a higher affinity for target
97 DNA sequences under oxidizing conditions than under reducing conditions (Cheng et al.,
98 2012; Ponnampalam et al., 1995). This change of binding affinity is caused by oxidative
99 modification of two conserved cysteine residues such as formation of an intramolecular
100 disulfide bond and/or to a sulfenic acid derivative (Cheng et al., 2012). Thus, PpsR functions
101 as both a redox and heme sensor.

102 Recently, we identified a novel persulfide sensor SqrR as a master regulator of
103 persulfide responsive genes which encode persulfide metabolic enzymes such as SQR,
104 sulfurtransferases and rhodanese homology domain proteins from the photosynthetic
105 bacterium *Rhodobacter capsulatus* (Shimizu et al., 2017). SqrR has two conserved cysteine
106 residues: Cys41 and Cys107 (Shimizu et al., 2017; Shimizu and Masuda, 2017). These
107 cysteine residues form an intramolecular tetrasulfide species when incubated with the sulfane
108 sulfur donor GSSH, resulting in reduced DNA binding affinity (Shimizu et al., 2017). SqrR
109 is a member of the arsenic repressor (ArsR) family of bacterial repressors, encoding a wide
110 range of metal, metalloid and non-metal sensing proteins (Busenlehner et al., 2003; Campbell
111 et al., 2007).

112 In this study, we provide evidence that SqrR binds heme and its DNA binding
113 affinity is reduced by the binding of heme. Furthermore, an increase in intracellular heme is
114 correlated with increased transcriptional levels of SqrR regulated genes. The potential
115 relationship between persulfide and heme in RSS signaling and metabolisms is discussed.

116

117 **Results**

118 *SqrR Binds Heme in vivo and in vitro*

119 To determine if SqrR binds to a cofactor like CstR, we purified FLAG-tagged SqrR from *R.*
120 *capsulatus*. To avoid contamination of the abundant photosynthetic apparatus containing
121 reaction center (RC), light harvesting (LH) 1 and 2, we disrupted the *pufBALMX* genes and

122 *pucBA* genes, which encode RC-LH1 and LH2 respectively, and the FLAG-tag was
123 integrated into the *sqrR* 3'-end coding sequence at its native chromosomal location. FLAG-
124 tagged SqrR was partially purified (Fig. 1A, arrow) and an absorption spectrum of this
125 protein preparation showed a peak at 416 nm as well as additional broad peaks in the 500-
126 650 nm region (Fig. 1B) implying binding of heme. Samples purified in the same way from
127 a FLAG-tagless *sqrR* strain, which does not contain SqrR-FLAG protein, did not show
128 absorbance (Fig. 1A and B), indicating that while the sample in Fig. 1B were not purified to
129 homogeneity, the absorption features observed were due to SqrR-FLAG. To test if the bound
130 substance was heme, and to determine the binding stoichiometry to the FLAG-tagged SqrR
131 protein, we performed an extraction on the purified protein with equal volume of 2% HCl in
132 acetone, following a specific heme quantification method (Masuda and Takahashi, 2006).
133 Separately, the FLAG-tagged SqrR protein concentration was measured by western blotting
134 using recombinant FLAG-tagged SqrR as a standard. As a result of these measurements, we
135 identified the binding substance is heme and estimated that $\approx 1.7\%$ of FLAG-tagged SqrR
136 purified from *R. capsulatus* binds heme under aerobic conditions in the absence of sulfide.

137 We subsequently tested whether the recombinant tagless SqrR, which was
138 overexpressed in *E. coli*, binds to heme. The absorption spectral changes of heme upon
139 addition of purified tagless SqrR were measured. Purified SqrR was incubated with 2-fold
140 excess of hemin (Fe(III) protoporphyrin IX complex) and un-bound hemin was removed by
141 size-exclusion chromatography (Yin et al., 2012). Although this filtration step allows removal
142 of 98% free hemin, the obtained protein containing fraction included hemin, indicating that
143 SqrR can interact with hemin. The absorption spectra of hemin and SqrR-bound hemin
144 (Heme-SqrR) were analyzed under oxidizing and reducing conditions (Fig. 1C and D). Under
145 oxidizing conditions, the Soret peak of hemin showed a broad doublet peak at 355 nm and
146 388 nm; however, the 388 nm Soret peak was dominant in that of Heme-SqrR (Fig. 1C and
147 D, black line). This Soret peak at 388 nm appears to be due to 5-coordinated thiolate-bound
148 Fe(III) heme (Smith et al., 2015). Moreover, the broad peak at around 620 nm clearly
149 indicates that a 5-coordinated high spin complex exists in the solution. Reduction of the
150 hemin-bound iron from Fe(III) to Fe(II) resulted in a shoulder Soret peak at 420 nm and
151 slightly different α and β peaks in the 510-610 nm in the spectrum of Heme-SqrR as
152 compared with that of hemin (Fig. 1C and D, red line). Although the visible band moved
153 from 620 nm to around 590 nm, the main peak is still located around 388 nm. Because Fe(II)
154 heme complexes with the Soret band around 388 nm are not known, this spectrum suggests

155 that an admixture of at least two heme coordination structures may exist. Additional
156 reconstitution assays with protoporphyrin IX showed that SqrR hardly binds the molecule,
157 suggesting specificity for heme (Supplementary Fig. 1).

158

159 The stoichiometry of heme binding to SqrR was addressed by reconstituting SqrR
160 with heme *in vitro*. To obtain the ratio of concentration at which SqrR becomes saturated
161 with heme, the relative absorbance of SqrR-heme to heme alone at 375 nm was plotted at
162 various protein:heme ratios (Fig. 1E and F). The plot of the absorbance change *versus* the
163 SqrR:heme concentration ratio was fitted by a one site binding model, and the obtained fit
164 indicated that the Heme-SqrR complex is formed with a $\approx 1:1$ SqrR to heme stoichiometry
165 (Fig. 1F). Tryptophan quenching data of heme titrated into SqrR can also be fitted with a one
166 site binding model with a K_d for heme binding of $0.442 \pm 0.058 \mu\text{M}$ (Fig. 1G). This value
167 was almost the same as $0.47 \pm 0.66 \mu\text{M}$ which is calculated by Fig. 1F. This micromolar
168 binding affinity is similar to a dissociation constant that has been reported for heme binding
169 by chlorite dismutase (Mayfield et al., 2013). While both titration experiments indicate
170 interaction with heme (Fig. 1F and G), we note that the binding constant derived from line
171 fitting may be an overestimate of the correct binding constant; because heme above
172 concentrations of ~ 400 nM oligomerizes.

173 Circular dichroism (CD) spectroscopy was employed to analyze structural change
174 of SqrR by the heme binding (Fig. 2). Based on the spectra obtained, secondary structure
175 contents were estimated by the BeStSel program (Table 1). The amount of α -helical
176 conformation in apo-SqrR was decreased by heme binding; the dithionite reduced and
177 oxidized Heme-SqrR showed 14.2% and 6.6% reduction of α -helical conformation,
178 respectively (Table 1). In contrast, β -sheet composition was increased in oxidized Heme-
179 SqrR (increased by 2.7%) and dithionite reduced Heme-SqrR (increased by 7.0%) when
180 compared with that in apo-SqrR. These results indicated that heme and its redox state affect
181 the secondary structure of SqrR. When dithionite reduced Heme-SqrR was reduced by DTT,
182 α -helical and β -sheet composition were increased by 11.7% and decreased by 7.4%,
183 respectively. This result indicated that reduction of cysteine thiol groups also affects the
184 structural change of the holo-SqrR. DTT-treated apo-SqrR showed a decrease in α -helical
185 composition and increase in β -sheet composition (Table 1). **Recently, the crystal structures**
186 **of reduced and di- or tetrasulfide formed C9S SqrR have been solved (Capdevila et al., 2020).**
187 **A comparative analysis of the reduced and disulfide formed C9S SqrR using the DSSP**

188 program (Kabsch and Sander, 1983) showed similar secondary structural changes to our
189 observation of the apo-SqrR and DTT-reduced apo-SqrR on CD spectroscopy. This similarity
190 implies that the native protein, and the C9S protein are structurally similar when the protein
191 is the reduced or oxidized states. As our results demonstrated that DTT-treated apo-SqrR
192 exhibited increased DNA-binding activity (Shimizu et al., 2017), these CD results suggest
193 that the DNA binding activity is modulated by structural changes. However, we note that
194 secondary structural changes just partially explain how DNA binding affinity is controlled
195 because the crystal structures indicated that the DNA-binding helices indeed were not
196 affected by redox state of conserved Cys41 and Cys107 (Capdevila et al., 2020).

197 To determine the amino acid residues which are utilized as axial ligands to the iron
198 of heme, we constructed point mutants of recombinant SqrR, where each candidate residue
199 was individually changed, and bound heme absorption spectra were compared for each SqrR.
200 We selected Cys9, Met17, His33, Met38, Cys41, Tyr88 and Cys107 as the candidate residue
201 because these residues (except for Cys9) were highly conserved in SqrR homologs from other
202 bacteria and Cys, Met, His and Tyr typically act as axial ligands in hemoproteins (Li et al.,
203 2011). We also constructed 15-amino acid N-terminal deletion mutant of SqrR (Δ N) to verify
204 the effect of acidic residues in N-terminal region on heme coordination because this region
205 is commonly conserved in SqrR homologs (Guimarães et al., 2011).

206 C9S SqrR showed similar absorption spectra to WT SqrR (Supplementary Fig. 2).
207 Because the redox state of Cys9 did not affect oxidative persulfidation between Cys41 and
208 Cys107 *in vitro* (Shimizu et al., 2017), it is likely that Cys9 does not contribute to heme
209 coordination. The absorption spectra of other point mutated SqrRs also showed a
210 coordination of heme similar to WT SqrR under oxidizing conditions (Fig. 3A, 3B,
211 Supplementary Fig. 2 and 3). On the other hand, only the dithionite reduced absorption
212 spectrum of C41S SqrR was different from that of WT SqrR (Fig 1D, Supplementary Fig. 4
213 and 5). The Soret peak showed a more prominent shoulder at 427 nm and the α and β peaks
214 were more separated than that of WT SqrR (Supplementary Fig. 5A, red line). The second-
215 order derivative absorption spectrum was different as indicated by arrows in Supplementary
216 Fig. 5C. The long wavelength peak of the doublet Soret peak was dominant and the α and β
217 peaks were distinctly separated. The frequency and intensity of the Soret band and α and β
218 peaks are known to be dependent on the electronic field of the fifth and sixth axial ligands of
219 the heme iron (Brill and Williams, 1961), and replacement of axial ligands causes spectral
220 changes in most hemoproteins (Block et al., 2007; Qi et al., 1999; Yin et al., 2012). Thus,

221 these observations imply that the Fe(II) heme complexes have an admixture of at least two
222 coordination species which was indicated by the double Soret peak (Fig. 1D) and Cys41
223 possibly forms an axial ligand under reducing conditions.

224 Heme binding affinity of the mutant protein was also different from the WT. The K_d
225 value for heme binding by C41S SqrR was $5.12 \pm 2.06 \mu\text{M}$ which is approximately 11-fold
226 higher than that of WT SqrR. This result further suggested that Cys41 is involved in SqrR-
227 heme coordination, and is similar to a prior case of a thiolate ligand mutation on a heme
228 binding protein, which resulted in a ~4-fold change of K_d value in the hemoprotein ATE1 (Hu
229 et al., 2008). We further tested the effect of cysteine reduction on axial ligand coordination
230 in WT SqrR because Cys41 and Cys107 is known to readily form a disulfide bond under
231 aerobic conditions (Shimizu et al., 2017). Heme-SqrR was treated with dithionite and
232 dithiothreitol (DTT) to reduce the iron of heme and the disulfide bond, respectively. The 416
233 nm Soret peak of dithionite and DTT treated Heme-SqrR (Fig. 1D, blue line) was more
234 dominant as compared with that of dithionite only treated Heme-SqrR (Fig. 1D, red line),
235 indicating that reduced Cys41 forms an axial ligand under disulfide and iron reducing
236 conditions. This 416 nm peak is coincident with that of FLAG-tagged SqrR from *R.*
237 *capsulatus* (Fig. 1B), implying that heme in SqrR is in the reduced form *in vivo*. Additionally,
238 we treated dithionite- and DTT-reduced WT and C41S Heme-SqrR with carbon monoxide
239 (CO) releasing reagent CORM-3 (Clark et al., 2003). The characteristic CO-heme spectra
240 with a Soret peak at 420 nm were observed in both WT and C41S Heme-SqrR
241 (Supplementary Fig. 6), implying that Cys41 of SqrR may form neutral thiol state.

242

243 *Heme Effects on DNA Binding Activity of SqrR*

244 Our previous study showed that SqrR forms an intramolecular tetrasulfide bond between
245 Cys41 and Cys107 when exposed to persulfide such as GSSH, which changes its DNA
246 binding affinity (Shimizu et al., 2017). To examine the effects of heme on binding activity of
247 SqrR, we characterized the interaction of SqrR with the *sqr* promoter region as the SqrR-
248 binding target. DNase I footprint analysis was undertaken with purified SqrR to confirm
249 whether the binding pattern to the *sqr* promoter region is different between SqrR and Heme-
250 SqrR or not (Fig. 3). Protection was observed and there was no significant difference between
251 SqrR and Heme-SqrR. We also performed the same analysis in the presence of dithionite in
252 order to verify the effect of reduction of heme on binding pattern; however, it showed same
253 binding pattern as compared with oxidized heme conditions (Supplementary Fig. 7).

254 We next assayed the binding affinity of SqrR for the promoter region by performing
255 gel mobility shift analysis with purified SqrR and a DNA probe of the *sqr* promoter. Heme
256 iron coordinates several molecules, *e.g.*, H₂O, O₂, CO, NO, CN⁻ and N₃⁻ (Toru Shimizu et
257 al., 2015). Sulfide (HS⁻) can also coordinate the iron of heme and it may cause production of
258 persulfide (Mishanina et al., 2015). It is possible that SqrR bound heme facilitates the
259 formation of tetrasulfide from sodium sulfide (Na₂S), and gel mobility shift analysis of
260 purified SqrR and Heme-SqrR was carried out with a DNA probe that encompasses the SqrR-
261 protected region in the *sqr* promoter. These assays were performed with untreated and fully
262 DTT-reduced SqrR as well as with SqrR treated with Na₂S. To avoid oxidation of Cys
263 residues by molecular oxygen, all experiments were carried out under anaerobic conditions.
264 SqrR and Heme-SqrR binds to the DNA probe in a concentration-dependent manner (Fig.
265 3A, B). Binding by SqrR in both the heme and non-heme bound forms was not altered by
266 Na₂S, indicating SqrR cannot form a tetrasulfide bond from Na₂S as previously described for
267 the non-heme form and heme does not contribute to persulfidation by sulfide (Fig. 3A,
268 B);(Shimizu et al., 2017). To investigate persulfide responsivity of Heme-SqrR, we carried
269 out the same analysis using Heme-SqrR reduced with DTT and Heme-SqrR treated with
270 GSSH which is an active persulfide sulfur donor for SqrR (Shimizu et al., 2017). The DNA
271 binding affinity of reduced Heme-SqrR is significantly greater (lower EC₅₀) than that of
272 GSSH-treated Heme-SqrR (Fig. 3C, Table 2), indicating that Heme-SqrR responds to
273 persulfide treatment in a similar way as to SqrR. However, the EC₅₀ value for Heme-SqrR
274 was ≈5.2-fold and ≈3.1-fold higher than that of SqrR under the reduced and GSSH-treated
275 conditions, respectively (Table 2). These experiments collectively reveal that heme does not
276 affect tetrasulfide bond formation but affects DNA binding affinity itself. Specifically, heme
277 binding lowers the promoter binding affinity of SqrR.

278

279 *An Increase in Heme is Associated with Transcriptional Induction of SqrR-regulated Genes* 280 *in Growing Cells*

281 In an attempt to gain *in vivo* insight into the above presented *in vitro* results, We measured
282 intracellular heme concentration during growth in the absence or presence of sulfide (Fig.
283 4A). Interestingly, heme concentration initially increased with growth in the absence of
284 sulfide. On the other hand, the addition of sulfide caused an initial decrease in the heme
285 concentration and a mild inhibition of heme synthesis. We confirmed that sulfide does not
286 prevent detection and quantification of heme with this method (Supplementary Fig. 8). We

287 also investigated *sqr* gene expression levels by qRT-PCR (Fig. 4B). After the addition of
288 sulfide, the transcriptional level increased as a result of SqrR sensing persulfide generated
289 from sulfide, resulting in loss of transcriptional repression activity (Shimizu et al., 2017). In
290 the absence of sulfide, the transcriptional level also increased despite the absence of sulfide,
291 consistent with the hypothesis that increased heme in the absence of sulfide results in SqrR-
292 dependent de-repression of the *sqr* gene in a heme-dependent manner. Consistent with this
293 hypothesis, *sqr* gene expression in a C41S (K_d heme = $5.12 \pm 2.06 \mu\text{M}$) mutant strain of *R.*
294 *capsulatus* was lower than that of WT ($0.442 \pm 0.058 \mu\text{M}$) (Fig. 4C).

295

296 **Discussion**

297 In this study we reveal that a persulfide-responsive transcriptional factor SqrR also
298 has a heme-responsive de-repression activity which can operate together with persulfide
299 responsivity. This conclusion is based on the observation that spectroscopic and biochemical
300 properties of SqrR were similar to well-known hemoprotein and heme-responsive
301 transcriptional factors, for example hemoprotein chlorite dismutase (Mayfield et al., 2013),
302 and bacterial heme sensor PpsR (Yin et al., 2012). SqrR purified from the host organism (*R.*
303 *capsulatus*) yielded weak spectroscopic features consistent with heme binding. The binding
304 of heme from this preparation was low (1.7%), which coincides with low de-repression at
305 this period of growth (Fig. 4A). However, when SqrR was purified from a heterologous host,
306 it could be reconstituted with hemin in an apparent $\approx 1:1$ stoichiometry (Fig. 1F). In addition,
307 the heterologously obtained protein exhibited a binding affinity towards hemin similar to
308 previously characterized proteins, and characterization of the C41S point mutation of the
309 protein suggested a possible axial cysteine involved in heme coordination.

310 An oxidized spectrum of heme binding SqrR is similar to several hemoproteins such
311 as Irr (Qi et al., 1999), chloroperoxidase (Sono et al., 1984) and hPer2 (Yang et al., 2008),
312 and the K_d value of SqrR for hemin is close to that of the hemoprotein chlorite dismutase
313 (Mayfield et al., 2013). CD spectroscopy indicated that hemin binding to SqrR led to a
314 decrease of the α -helical secondary structure (Fig. 2 and Table 1). Such conformational
315 change had been reported in the cyanobacterial heme-responsive transcriptional factor FurA,
316 where a decrease in α -helix contents caused by heme binding was found to negatively affect
317 DNA binding affinity (Pellicer et al., 2012). The DNA binding affinity of SqrR to target
318 promoter regions is decreased by the binding of hemin (Fig. 3C and Table 2), similar to other
319 bacterial heme sensors such as PpsR (Yin et al., 2012) and HrtR (Sawai et al., 2012). These

320 results suggest that SqrR also binds to heme and changes its activity *in vitro*.

321 Although still tentative, we consider that Fe(II) heme possibly binds to SqrR *in vivo*
322 since the 416 nm Soret peak was same between dithionite- and DTT-treated Heme-SqrR (Fig.
323 1D, blue line) and FLAG-tagged SqrR from *R. capsulatus* (Fig. 1B). It is likely that Cys41
324 may be involved in coordination of Fe(II) heme (Supplementary Fig. 5). Typically, thiolate
325 of cysteine coordinates to iron of heme by either the thiolate (RS⁻) or neutral thiol form (RSH)
326 (Kühl and Imhof, 2014; Shimizu, 2012; Smith et al., 2015). In small-molecule
327 sensors/transporters such as heme-regulated eIF2 α kinase, Cys-Pro sequence (CP motif) is
328 possibly critical for Fe(III) heme binding and amino acid residues other than cysteine such
329 as histidine bind to Fe(II) heme nonspecifically (Igarashi et al., 2008; Shimizu, 2012). In
330 enzymes such as cytochrome P450 and nitric oxide synthase, thiolate cysteine can coordinate
331 both Fe(III) and Fe(II) heme (Shimizu, 2012; Smith et al., 2015). SqrR does not have CP
332 motif and Cys41 might coordinate to Fe(II) heme and not Fe(III) heme (Supplementary Fig.
333 5B and C); therefore, the coordination character of Cys41-Fe(II) heme is possibly similar to
334 cytochrome P450. Interestingly, a spectrum of reduced, CO-bound Heme-SqrR showed a
335 peak at 420 nm (Supplementary Fig. 6), although thiolate-bound Fe(II)-CO heme in
336 cytochrome P450 shows a peak at 450 nm. It is reported that either His or neutral thiol
337 (protonated Cys) is the internal axial ligand for the CO-Fe(II) heme complex of P420 (Sabat
338 et al., 2009; Sono et al., 2018; Sun et al., 2013). Indeed, the spectrum of the Fe(II)-CO heme
339 complex of H93G myoglobin shows a peak at 420 nm based on coordination by neutral thiol
340 to Fe(II)-CO heme (Sabat et al., 2009). Together, these reports imply that Cys41 of SqrR may
341 form neutral thiol state.

342 Spectral analysis indicated that several coordination states in C41S SqrR under
343 reduced conditions existed (Supplementary Fig. 5), implying that amino acid residues other
344 than Cys41 may form an axial ligand. Moreover, oxidized WT SqrR, which forms a disulfide
345 bond between Cys41 and Cys107, can bind to hemin (Fig. 1D). The crystal structure of SqrR
346 homolog, BigR, showed that two methionine residues (Met17 and Met38) are close at Cys41
347 (Guimarães et al., 2011); therefore, a part of Met17 and/or Met38 in SqrR may also
348 coordinate to Fe(II) heme. Indeed, M38K SqrR showed a slightly higher peak at 427 nm as
349 compared with that of WT SqrR under reducing conditions (Supplementary Fig. 4).

350 The DNA binding affinity of GSSH treated Heme-SqrR was lower than both that of
351 SqrR and GSSH treated SqrR (Table 2), indicating that Heme-SqrR can likely form a
352 tetrasulfide bond while heme is retained in SqrR. In several hemoproteins, heme-binding is

353 regulated by thiol/disulfide redox switch (Ragsdale and Yi, 2010). Oxidized heme
354 oxygenase-2 (HO-2), which contains an intramolecular disulfide bond, binds heme tightly,
355 whereas heme-binding affinity of HO-2 is decreased by reduction of disulfide bond (Yi and
356 Ragsdale, 2007). The decrease in DNA-binding affinity by Heme-SqrR was greater in
357 reduced SqrR (≈ 5.2 -fold) than in GSSH-treated SqrR (≈ 3.1 -fold) (Table 2). This may indicate
358 that the effect of heme on DNA-binding affinity is modulated by the thiol oxidation state.
359 Moreover, in a heme-binding nuclear hormone receptor, reversible formation of a disulfide
360 bond and thiolate-bound Fe(III) heme through the same cysteine residue is altered by redox
361 state (Gupta and Ragsdale, 2011). Such switching is likely to occur in Cys41 of SqrR, since
362 both reduced and GSSH-treated SqrR binds to heme.

363 Our *in vivo* data showed that an increase in intracellular heme concentration is
364 correlated with loss of the transcriptional repression by SqrR (Fig. 4), although the change
365 and effect of heme were small. Indeed, only 1.7% of purified SqrR-FLAG binds heme in *R.*
366 *capsulatus* (Fig. 1A), suggesting that SqrR exclusively senses RSS, but not heme, *in vivo*.
367 However, our *in vitro* data evidently showed that SqrR binds heme at a near one-to-one ratio
368 with a binding constant similar to other heme-binding proteins, suggesting the still tentative
369 hypothesis of heme-sensing by SqrR *in vivo*. Why can SqrR sense both persulfide and heme?
370 In mitochondria, a heme-dependent sulfide oxidation pathway is proposed (Mishanina et al.,
371 2015). In this pathway, a sulfide anion binds to ferric heme of hemoproteins such as
372 hemoglobin and persulfidation occurs by reaction with several sulfide anions (Galardon et
373 al., 2017; Mishanina et al., 2015). Intracellular free heme might be capable of similar catalytic
374 activity. Moreover, hemoproteins are also known to function as hydrogen sulfide transport
375 proteins in invertebrates living in sulfide-rich habitats (Kraus et al., 1990; Kraus and
376 Wittenberg, 1990). Intracellular heme might also be able to act as a sulfide carrier in the
377 presence of an excess of sulfide, therefore, when cells are exposed to sulfide it may be
378 effective to express heme efflux systems as well as a RSS metabolic pathway in order to
379 remove toxic RSS rapidly. Thus, the amount of persulfide may be linked to that of heme. In
380 *R. capsulatus*, although the intracellular heme concentration is decreased by treatment of
381 cells with sulfide (Fig. 4A), the relationship between persulfide and heme is unclear.
382 Moreover, it is considered that SqrR homolog, BigR, does not function as a metal sensor
383 (Guimarães et al., 2011). The ability of SqrR to function as both persulfide and heme sensor
384 may thus be valuable for improving RSS related metabolic dynamics. Overall, we consider
385 that SqrR predominantly functions as persulfide sensor and the effect of heme on the activity

386 could be helpful to respond to RSS in specific environmental conditions. Further elucidation
387 of the physiological role(s) and response of heme-related proteins in this and other organisms,
388 promises a better understanding of the RSS response and the metabolism of heme.

389

390 **Materials and Methods**

391 *Bacterial Strains, Media, and Growth Conditions*

392 *E. coli* strains JM109/ λ pir, S17-1/ λ pir and BL21 (DE3) were used for cloning, conjugal
393 transfer of plasmids, and protein overexpression, respectively. *E. coli* cells were routinely
394 grown in Luria Bertani (LB) medium at 37°C. Kanamycin and gentamycin were used at a
395 concentration of 50 μ g/mL, 10 μ g/mL, respectively.

396 *R. capsulatus* strain SB1003 and mutant strains were grown under aerobic-dark
397 (aerobic) condition at 30°C in PYS medium, as described previously (Nagashima et al., 1997).
398 Gentamycin and rifampicin were used at a concentration of 1.5 μ g/mL and 75 μ g/mL,
399 respectively.

400

401 *Purification of SqrR from R. capsulatus*

402 Two 500-bp DNA fragments consisting of the N-terminal and C-terminal regions of
403 *pufBALMX* operon and *pucBA* operon were amplified by PCR with Prime STAR HS
404 polymerase (TaKaRa). Two sets of primers were used for amplification. One set contained
405 forward primer puffer1 (5'-TTGCATGCAACACCCGGTTCTGACACGGATTTCCGG-3')
406 and the reverse primer pufrev1 (5'-TTTTGATATCGTTCTTATCAGCCATAACAACCTCC-
407 3') or forward primer pucfor1 (5'-
408 TTGCATGCGCGGACAATTCGACCTGAAAATTCCG-3') and the reverse primer
409 pucrev1 (5'-TTTTGATATCTTTATCGTCAGTCATTGTCCCGAAT-3'), respectively. The
410 other set contained forward primer puffer1 (5'-
411 TTTTGATATCACCGAAGTCGTCTGACACCGCTTTC-3') and the reverse primer
412 pufrev2 (5'-TTGGATCCGGCTCTCGGAGCGTTTCGGAAAGCCCG-3') or forward
413 primer pucfor2 (5'-TTTTGATATCGCGCCGGCTCAGTAATCTGCTGACC-3') and the
414 reverse primer pucrev2 (5'-TTGGATCCGCTCATTCCGATCCAGCGCGGCGCATC-3'),
415 respectively. Each fragments were cloned into pZJD29a (Masuda and Bauer, 2004) and
416 obtained plasmids were used for deletion of *pufBALMX* and *pucBA* genes in *R. capsulatus*
417 Δ *sqrR* strain as described previously (Shimizu et al., 2017). FLAG-tagged *sqrR* was
418 transferred to *R. capsulatus* Δ *sqrR*, Δ *pufBALMX* and Δ *pucBA* triple mutant as described

419 previously (Shimizu et al., 2017). 1L of SqrR-FLAG strain culture grown under aerobic
420 conditions was collected and resuspended in lysis buffer (50 mM Tris-HCl, pH 7.4, 150 mM
421 NaCl, 1 mg/ml lysozyme, and 1/100 vol. Protease Inhibitor Cocktail (Nacalai)). Cells were
422 kept on ice, disrupted by sonication of 10 sec with 10 sec interval, for 10 min in total. Lysed
423 cells were centrifuged at 15000 x g for 30 min, and the filtered supernatant was incubated
424 with anti-FLAG M2 affinity gel (Sigma) at 4°C overnight. The anti-FLAG gel was spun
425 down and washed with TBS buffer (50 mM Tris-HCl, pH 7.4, 150 mM NaCl). SqrR-FLAG
426 was eluted with 3xFLAG peptide (Protein Ark). For quantifying concentration of SqrR-
427 FLAG, recombinant FLAG-tagged SqrR was purified from *E. coli* (see below) to use as a
428 standard. A standard curve of FLAG-tagged SqrR was obtained by measuring signal intensity
429 of Western blotting using anti-FLAG antibody and the concentration of SqrR-FLAG purified
430 from *R. capsulatus* was determined.

431

432 *Overexpression and Purification of WT and Mutant SqrR from E. coli*

433 Recombinant SqrR was overexpressed in *E. coli* strain BL21 (DE3) using pSUMO::SqrR
434 plasmid, which was constructed in a previous study (Shimizu et al., 2017), by induction with
435 0.2 mM isopropyl- β -D-thiogalactopyranoside (IPTG) at 16°C overnight (12-16 h). Each
436 point mutation was subsequently introduced by a standard PCR mutagenesis method with the
437 pSUMO::SqrR plasmid used as a PCR template (Vandeyara et al., 1988). For construction of
438 Δ N SqrR, pSUMO::SqrR lacking N-terminal 15 A.A. was amplified by PCR with a forward
439 primer (5'- GAGGACATGAAATGGCGACACGGGCGCGGGCGGCC-3') and a reverse
440 primer (5'- CCATTTTCATGTCCTCCAATCTGTTCGCGGTGAGCC-3') and the amplified
441 DNA was self-ligated by In-Fusion HD Cloning kit (Clontech). For construction of SqrR-
442 FLAG, the DNA fragment of FLAG-tagged *sqrR* gene was amplified by PCR using
443 pZJD3::SqrR-FLAG plasmid, which was constructed in a previous study (Shimizu et al.,
444 2017), as a template with a forward primer (5'-
445 AGATTGGAGGACATATGGGGTCCGACACGGACGAG-3') and a reverse primer (5'-
446 GTCCGCGGTACCATATCACTTATCATCATCCT-3') and the amplified DNA was
447 cloned into the *Nde*I-cut pSUMO vector by In-Fusion HD Cloning kit (Clontech). The
448 obtained plasmids for overexpression of point mutants of SqrR were also transferred into *E.*
449 *coli* strain BL21 (DE3) and overexpressed by the same procedure. Wild type (WT) SqrR and
450 mutant SqrR were purified essentially as described previously (Shimizu et al., 2017).

451

452 *Hemin-SqrR Interaction*

453 Hemin (Sigma) stock solutions were freshly dissolved in 0.01 M NaOH. The final
454 concentration was determined spectrophotometrically using a coefficient of $58.4 \text{ mM}^{-1} \text{ cm}^{-1}$
455 (Dawson, R. M., Elliott, D. C., Elliot, W. H., and Jones, 1969). Purified recombinant SqrR
456 was incubated with a 2-fold excess of hemin at room temperature for 20 min (Yin et al., 2012).
457 The unbound hemin was then removed by passing through PD MidiTrapTM G-25 column (GE
458 Healthcare) with 20 mM Tris-HCl (pH 8.0), 500 mM NaCl, 6% Glycerol. For analyzing
459 interaction with protoporphyrin IX (Sigma), the stock solution was prepared by solubilizing
460 in DMSO and SqrR was treated by the same method as with hemin.

461

462 *Spectrophotometric Measurements*

463 Absorption Ultraviolet (UV)-visible spectra were recorded using a spectrophotometer UV-
464 1800 (SHIMADZU). To measure the oxidized and reduced spectrum, excess sodium
465 ferricyanide in solution and a few grains of solid dithionite was added to samples,
466 respectively. To measure the Fe-CO Heme spectra, dithionite- and DTT-reduced Heme-SqrR
467 was treated with 100 μM tricarbonylchloro(glycinato)ruthenium(II) (CORM-3) (Clark et al.,
468 2003) and then spectrum was recorded immediately.

469

470 *Tryptophan Fluorescence Quenching Assays*

471 Fluorescence measurements were performed at room temperature using a Fluorescence
472 Spectrophotometer F-2700 (Hitachi) in a 2 ml sample volume with 1 μM recombinant SqrR
473 in 20 mM Tris-HCl (pH 8.0), 500 mM NaCl, 6% glycerol. Hemin was added into the sample
474 to a final concentration of 0.1-2.7 μM . After incubation for 2 min, the sample was excited at
475 280 nm. Three emissions from 290 to 400 nm were then recorded and averaged. Data were
476 processed using nonlinear curve fitting with a one site binding model using an in-house fitting
477 software (Arai et al., 2012).

478

479 *Circular dichroism (CD) spectroscopy*

480 CD spectra were measured in a JASCO J-805 spectropolarimeter (JASCO, Tokyo, Japan) at
481 200-250 nm with a quartz cuvette of 1 mm path length at 25°C (controlled by a thermostat
482 circulating water bath). Analysis was performed using recombinant SqrR at a protein
483 concentration of 0.2 mg/mL which was determined by Bradford assay.

484

485 *DNase I Footprint Assay*

486 The 6-FAM-labeled DNA probe consisting of the *sqr* promoter region was prepared by PCR
487 Footprint analysis was performed as described previously (Takayuki Shimizu et al., 2015).
488 For reducing the iron of hemin, protein was treated by dithionite before analysis under
489 aerobic conditions.

490

491 *Gel Mobility Shift Analysis*

492 A Cy5-labeled 200-bp DNA probe corresponding to the *sqr* promoter region was purified as
493 described previously and used as a probe for the gel shift analysis (Shimizu et al., 2017).
494 When anaerobic conditions were required, all buffers were degassed and all processes were
495 carried out in an anaerobic globe box. Reduced SqrR was prepared by treating with 5 mM
496 DTT, followed by gel filtration (to remove DTT) under anaerobic conditions. When
497 (per)sulfide treatment was required, SqrR was anaerobically incubated (30 min, room
498 temperature) with a 5-fold S:cysteine thiol excess of Na₂S or GSSH. GSSH was freshly
499 prepared by chemosynthesis of a five-fold molar excess of freshly dissolved Na₂S with
500 glutathione disulfide as described previously (Shimizu et al., 2017).

501

502 *Quantification of Intracellular Heme Concentration*

503 *R. capsulatus* was grown aerobically to mid-log phase in PYS medium. For sulfide treatment,
504 a final 0.6 mM of Na₂S was added and cells were further grown for 0, 30, 60, 90, 120 and
505 240 min. At each time point, an amount of cells that corresponded to an OD₆₆₀=1.0 per ml
506 was used for determination of intracellular heme concentration. Cells were washed and
507 resuspended with filtered 100 mM Tris-HCl (pH 8.4) and then disrupted by sonication.
508 Disrupted cells were centrifuged at 15000 x g for 30 min, and the supernatant was used for
509 measurement. For SqrR-FLAG solution, equal volume of acetone peroxide was added and
510 mixture was centrifuged at 15000 x g for 10 min, and the supernatant was used for
511 measurement. Reaction mixtures contained final concentrations of 250 nM horseradish
512 peroxidase (HRP) apo-enzyme (Blaenavon, Wales), 100 mM Tris-HCl (pH 8.4), and the
513 supernatant or hemin solution (range 125-1000 pM in serial dilution) as a standard was
514 prepared to bring the final volume of each sample to 100 µl and incubated for 30 min at room
515 temperature for reconstitution of active HRP. Peroxidase activities were assayed using ECL
516 Prime Western Blotting Detection Reagent (GE healthcare). Assay mixture (100 µl) was
517 added to the reaction mixture. After 2 min incubation at room temperature, chemiluminescent

518 intensity was measured using a ImageQuant LAS 500 (GE healthcare).

519

520 *RNA Isolation and Quantitative Real-Time PCR (qRT-PCR)*

521 *R. capsulatus* was grown and harvested in the same procedure as sampling for quantification
522 of intracellular heme concentration. 0.5 ml of cells were harvested with total RNA of each
523 sample extracted using SV Total RNA Isolation System (Promega). A typical OD₂₆₀ to OD₂₈₀
524 ratio of RNA sample was approximately 2.0. Reverse transcription was performed using
525 PrimeScript RT Reagent kit (TaKaRa). cDNA was amplified using SYBR PreMix Ex Taq
526 (TaKaRa). Signal detection and quantification were performed in duplicate using the Thermal
527 Cycler Dice Real Time System (TaKaRa). As an internal control, the house-keeping gene
528 *rpoZ* that encodes DNA-directed RNA polymerase omega subunit was used with the
529 following gene-specific primers:

530 *rpoZ*for: 5'-GAGATCGCCGATGAAACC-3'

531 *rpoZ*rev: 5'-TCGTCGACCTCGATCTGG-3'

532 *sqr*for: 5'-CGCAAGGAAGACAAGGTCAC-3'

533 *sqr*rev: 5'-CGAGGGCACGAAATGATAC-3'

534

535 **Funding information**

536 This work was supported by the Japan Science Society Sasakawa Fellowship [to T.S.], the
537 Opto Science Foundation [to S.E.M.], Ohsumi Frontier Science Foundation [to S.M.], and
538 the Japan Society for Promotion of Science [KAKENHI (18K14650, 18H03941) to T.S.,
539 (18K05386) to Y.H., (19H02521) to M.A., (18H03941, 20K06681) to T.M. and
540 (19H04719) to S.M.].

541

542 **Disclosures**

543 Conflicts of interest: No conflicts of interest declared.

544

545 **Acknowledgments**

546 We thank Prof. Takafumi Ueno and Dr. Satoshi Abe at the Tokyo Institute of Technology
547 for discussion of interpreting the absorption spectrum.

548

549 **References**

550 Akaike, T., Ida, T., Wei, F.-Y., Nishida, M., Kumagai, Y., Alam, M.M., et al. (2017)

551 CysteinyI-tRNA synthetase governs cysteine polysulfidation and mitochondrial
552 bioenergetics. *Nature communications*. 8: 1177.

553 Arai, M., Ferreon, J.C., and Wright, P.E. (2012) Quantitative analysis of multisite protein-
554 ligand interactions by NMR: Binding of intrinsically disordered p53 transactivation
555 subdomains with the TAZ2 domain of CBP. *Journal of the American Chemical
556 Society*. 134: 3792–3803.

557 Aroca, A., Schneider, M., Scheibe, R., Gotor, C., and Romero, L.C. (2017) Hydrogen
558 sulfide regulates the cytosolic/nuclear partitioning of glyceraldehyde-3-phosphate
559 dehydrogenase by enhancing its nuclear localization. *Plant and Cell Physiology*. 58:
560 983–992.

561 Birke, H., De Kok, L.J., Wirtz, M., and Hell, R. (2015) The role of compartment-specific
562 cysteine synthesis for sulfur homeostasis during H₂S exposure in Arabidopsis. *Plant
563 and Cell Physiology*. 56: 358–367.

564 Block, D.R., Lukat-Rodgers, G.S., Rodgers, K.R., Wilks, A., Bhakta, M.N., and Lansky,
565 H.B. (2007) Identification of two heme-binding sites in the cytoplasmic heme-
566 trafficking protein PhuS from *Pseudomonas aeruginosa* and their relevance to
567 function. *Biochemistry*. 46: 14391–14402.

568 Brill, A.S., and Williams, R.J.P. (1961) The absorption spectra, magnetic moments and the
569 binding of iron in some haemoproteins. *Biochemical journal*. 78: 246–253.

570 Busenlehner, L.S., Pennella, M.A., and Giedroc, D.P. (2003) The SmtB/ArsR family of
571 metalloregulatory transcriptional repressors: Structural insights into prokaryotic metal
572 resistance. *FEMS Microbiology Reviews*. 27: 131–143.

573 Campbell, D.R., Chapman, K.E., Waldron, K.J., Tottey, S., Kendall, S., Cavallaro, G., et al.
574 (2007) Mycobacterial cells have dual nickel-cobalt sensors: Sequence relationships
575 and metal sites of metal-responsive repressors are not congruent. *Journal of Biological
576 Chemistry*. 282: 32298–32310.

577 Capdevila, D.A., Walsh, B.J.C., Zhang, Y., Dietrich, C., Gonzalez-gutierrez, G., and
578 Giedroc, D.P. (2020) Structural basis for persulfide-sensing specificity in a
579 transcriptional regulator. *Nature Chemical Biology*. [https://doi.org/10.1038/s41589-
580 020-00671-9](https://doi.org/10.1038/s41589-020-00671-9)

581 Chang, F.M.J., Coyne, H.J., Cubillas, C., Vinuesa, P., Fang, X., Ma, Z., et al. (2014) Cu(I)-
582 mediated allosteric switching in a copper-sensing operon repressor (CsoR). *Journal of
583 Biological Chemistry*. 289: 19204–19217.

584 Chen, W., Rosser, E.W., Matsunaga, T., Pacheco, A., Akaike, T., and Xian, M. (2015) The
585 development of fluorescent probes for visualizing intracellular hydrogen polysulfides.
586 *Angew Chem Int Ed Engl.* 54: 13961–13965.

587 Chen, Z., Huang, Y., Yang, W., Chang, G., Li, P., Wei, J., et al. (2019) The hydrogen
588 sulfide signal enhances seed germination tolerance to high temperatures by retaining
589 nuclear COP1 for HY5 degradation. *Plant Science.* 285: 34–43.

590 Cheng, Z., Wu, J., Setterdahl, A., Reddie, K., Carroll, K., Hammad, L.A., et al. (2012)
591 Activity of the tetrapyrrole regulator CrtJ is controlled by oxidation of a redox active
592 cysteine located in the DNA binding domain. *Molecular Microbiology.* 85: 734–746.

593 Clark, J.E., Naughton, P., Shurey, S., Green, C.J., Johnson, T.R., Mann, B.E., et al. (2003)
594 Cardioprotective Actions by a Water-Soluble Carbon Monoxide–Releasing Molecule.
595 *Circulation Research.* 93: 1–7.

596 Cuevasanta, E., Lange, M., Bonanata, J., Coitiño, E.L., Ferrer-Sueta, G., Filipovic, M.R., et
597 al. (2015) Reaction of hydrogen sulfide with disulfide and sulfenic acid to form the
598 strongly nucleophilic persulfide. *Journal of Biological Chemistry.* 290: 26866–26880.

599 Dawson, R. M., Elliott, D. C., Elliot, W. H., and Jones, K.M. (1969) Data for Biochemical
600 Research, 2nd Ed. p.316, Oxford University Press, Oxford.

601 Dóka, É., Pader, I., Bíró, A., Johansson, K., Cheng, Q., Ballagó, K., et al. (2016) A novel
602 persulfide detection method reveals protein persulfide- and polysulfide-reducing
603 functions of thioredoxin and glutathione systems. *Science advances.* 2: e1500968.

604 Galardon, E., Huguet, F., Herrero, C., Ricoux, R., Artaud, I., and Padovani, D. (2017)
605 Reactions of persulfides with the heme cofactor of oxidized myoglobin and
606 microperoxidase 11: reduction or coordination. *Dalton Trans.* 46: 7939–7946.

607 Guimarães, B.G., Barbosa, R.L., Soprano, A.S., Campos, B.M., De Souza, T.A., Tonoli,
608 C.C.C., et al. (2011) Plant pathogenic bacteria utilize biofilm growth-associated
609 repressor (BigR), a novel winged-helix redox switch, to control hydrogen sulfide
610 detoxification under hypoxia. *Journal of Biological Chemistry.* 286: 26148–26157.

611 Gupta, N., and Ragsdale, S.W. (2011) Thiol-disulfide redox dependence of heme binding
612 and heme ligand switching in nuclear hormone receptor Rev-erb β . *Journal of*
613 *Biological Chemistry.* 286: 4392–4403.

614 Hu, R.-G., Wang, H., Xia, Z., and Varshavsky, A. (2008) The N-end rule pathway is a
615 sensor of heme. *Proceedings of the National Academy of Sciences.* 105: 76–81.

616 Ida, T., Sawa, T., Ihara, H., Tsuchiya, Y., Watanabe, Y., Kumagai, Y., et al. (2014)

617 Reactive cysteine persulfides and S-polythiolation regulate oxidative stress and redox
618 signaling. *Proceedings of the National Academy of Sciences of the United States of*
619 *America*. 111: 7606–11.

620 Igarashi, J., Murase, M., Iizuka, A., Pichierri, F., Martinkova, M., and Shimizu, T. (2008)
621 Elucidation of the heme binding site of heme-regulated eukaryotic initiation factor 2 α
622 kinase and the role of the regulatory motif in heme sensing by spectroscopic and
623 catalytic studies of mutant proteins. *Journal of Biological Chemistry*. 283: 18782–
624 18791.

625 Kabsch, W., and Sander, C. (1983) Dictionary of protein secondary structure: Pattern
626 recognition of hydrogen-bonded and geometrical features. *Biopolymers*. 22: 2577–
627 2637.

628 Kraus, D.W., and Wittenberg, J.B. (1990) Hemoglobins of the *Lucina pectinata* /bacteria
629 symbiosis. 1. Molecular properties, kinetics and equilibria of reactions with ligands.
630 *Journal of Biological Chemistry*. 265: 16043–16053.

631 Kraus, D.W., Wittenberg, J.B., Lu, J.F., and Peisach, J. (1990) Hemoglobins of the *Lucina*
632 *pectinata*/bacteria symbiosis. 2. An electron paramagnetic resonance and optical
633 spectral study of the ferric proteins. *Journal of Biological Chemistry*. 265: 16054–
634 16059.

635 Kühl, T., and Imhof, D. (2014) Regulatory Fe^{II/III} heme: The reconstruction of a molecule's
636 biography. *ChemBioChem*. 15: 2024–2035.

637 Li, J., Chen, S., Wang, X., Shi, C., Liu, H., Yang, J., et al. (2018) Hydrogen Sulfide
638 Disturbs Actin Polymerization via S-Sulfhydration Resulting in Stunted Root Hair
639 Growth. *Plant physiology*. 178: 936–949.

640 Li, T., Bonkovsky, H.L., and Guo, J. (2011) Structural analysis of heme proteins:
641 implications for design and prediction. *BMC Structural Biology*. 11: 13.

642 Li, Z.G., Min, X., and Zhou, Z.H. (2016) Hydrogen sulfide: A signal molecule in plant
643 cross-adaptation. *Frontiers in Plant Science*. 7: 1621.

644 Libiad, M., Yadav, P.K., Vitvitsky, V., Martinov, M., and Banerjee, R. (2014) Organization
645 of the human mitochondrial hydrogen sulfide oxidation pathway. *Journal of*
646 *Biological Chemistry*. 289: 30901–30910.

647 Luebke, J.L., Arnold, R.J., and Giedroc, D.P. (2013) Selenite and tellurite form mixed
648 seleno- and tellurotrisulfides with CstR from *Staphylococcus aureus*. *Metallomics :*
649 *integrated biometal science*. 5: 335–42.

650 Luebke, J.L., Shen, J., Bruce, K.E., Kehl-Fie, T.E., Peng, H., Skaar, E.P., et al. (2014) The
651 CsoR-like sulfurtransferase repressor (CstR) is a persulfide sensor in *Staphylococcus*
652 *aureus*. *Molecular Microbiology*. 94: 1343–1360.

653 Masuda, S., and Bauer, C.E. (2004) Null Mutation of HvrA Compensates for Loss of an
654 Essential *relA/spoT*-Like Gene in *Rhodobacter capsulatus*. *Journal of Bacteriology*.
655 186: 235–239.

656 Masuda, T., and Takahashi, S. (2006) Chemiluminescent-based method for heme
657 determination by reconstitution with horseradish peroxidase apo-enzyme. *Analytical*
658 *Biochemistry*. 355: 307–309.

659 Mayfield, J.A., Hammer, N.D., Kurker, R.C., Chen, T.K., Ojha, S., Skaar, E.P., et al.
660 (2013) The chlorite dismutase (HemQ) from *Staphylococcus aureus* has a redox-
661 sensitive heme and is associated with the small colony variant Phenotype *. *Journal of*
662 *Biological Chemistry*. 288: 23488–23504.

663 Micsonai, A., Wien, F., Kernya, L., Lee, Y.-H., Goto, Y., Réfrégiers, M., et al. (2015)
664 Accurate secondary structure prediction and fold recognition for circular dichroism
665 spectroscopy. *Proceedings of the National Academy of Sciences*. 112: E3095–E3103.

666 Mishanina, T. V, Libiad, M., and Banerjee, R. (2015) Biogenesis of reactive sulfur species
667 for signaling by hydrogen sulfide oxidation pathways. *Nature Chemical Biology*. 11:
668 457–464.

669 Mustafa, A.K., Gadalla, M.M., Sen, N., Kim, S., Mu, W., Sadia, K., et al. (2009) H₂S
670 signals through protein S-sulfhydration. *Science signaling*. 2: ra72.

671 Nagashima, K. V, Hiraishi, A., Shimada, K., and Matsuura, K. (1997) Horizontal transfer
672 of genes coding for the photosynthetic reaction centers of purple bacteria. *Journal of*
673 *molecular evolution*. 45: 131–136.

674 Nishida, M., Sawa, T., Kitajima, N., Ono, K., Inoue, H., Ihara, H., et al. (2012) Hydrogen
675 sulfide anion regulates redox signaling via electrophile sulfhydration. *Nature*
676 *Chemical Biology*. 8: 714–724.

677 Ono, K., Akaike, T., Sawa, T., Kumagai, Y., Wink, D.A., Tantillo, D.J., et al. (2014) Redox
678 chemistry and chemical biology of H₂S, hydropersulfides, and derived species:
679 Implications of their possible biological activity and utility. *Free Radical Biology and*
680 *Medicine*. 77: 82–94.

681 Pellicer, S., González, A., Peleato, M.L., Martinez, J.I., Fillat, M.F., and Bes, M.T. (2012)
682 Site-directed mutagenesis and spectral studies suggest a putative role of FurA from

683 *Anabaena* sp. PCC 7120 as a heme sensor protein. *FEBS Journal*. 279: 2231–2246.
684 Ponnampalam, S.N., Buggy, J.J., and Bauer, C.E. (1995) Characterization of an aerobic
685 repressor that coordinately regulates bacteriochlorophyll, carotenoid, and light
686 harvesting-II expression in *Rhodobacter capsulatus*. *Journal of Bacteriology*. 177:
687 2990–2997.

688 Qi, Z., Hamza, I., and O’Brian, M.R. (1999) Heme is an effector molecule for iron-
689 dependent degradation of the bacterial iron response regulator (Irr) protein.
690 *Proceedings of the National Academy of Sciences of the United States of America*. 96:
691 13056–13061.

692 Ragsdale, S.W., and Yi, L. (2010) Thiol/Disulfide Redox Switches in the Regulation of
693 Heme Binding to Proteins. *Antioxidants & Redox Signaling*. 14: 1039–1047.

694 Sabat, J., Stuehr, D.J., Yeh, S.-R., and Rousseau, D.L. (2009) Characterization of the
695 Proximal Ligand in the P420 Form of iNOS. *J Am Chem Soc*. 131: 12186.

696 Sawai, H., Yamanaka, M., Sugimoto, H., Shiro, Y., and Aono, S. (2012) Structural basis
697 for the transcriptional regulation of heme homeostasis in *Lactococcus lactis*. *Journal*
698 *of Biological Chemistry*. 287: 30755–30768.

699 Shatalin, K., Shatalina, E., Mironov, A., and Nudler, E. (2011) H₂S: A universal defense
700 against antibiotics in bacteria. *Science*. 334: 986–990.

701 Shen, J., Peng, H., Zhang, Y., Trinidad, J.C., and Giedroc, D.P. (2016) *Staphylococcus*
702 *aureus* *sqr* encodes a type II sulfide:quinone oxidoreductase and impacts reactive
703 sulfur speciation in cells. *Biochemistry*. 55: 6524–6534.

704 Shimizu, T. (2012) Binding of cysteine thiolate to the Fe(III) heme complex is critical for
705 the function of heme sensor proteins. *Journal of inorganic biochemistry*. 108: 171–
706 177.

707 Shimizu, Takayuki, Cheng, Z., Matsuura, K., Masuda, S., and Bauer, C.E. (2015) Evidence
708 that altered *cis* element spacing affects PpsR mediated redox control of photosynthesis
709 gene expression in *Rubrivivax gelatinosus*. *PLoS ONE*. 10: e0128446.

710 Shimizu, Toru, Huang, D., Yan, F., Stranova, M., Bartosova, M., Fojtíková, V., et al.
711 (2015) Gaseous O₂, NO, and CO in Signal Transduction: Structure and Function
712 Relationships of Heme-Based Gas Sensors and Heme-Redox Sensors. *Chemical*
713 *Reviews*. 115: 6491–6533.

714 Shimizu, T., and Masuda, S. (2017) Characterization of redox-active cysteine residues of
715 persulfide-responsive transcriptional repressor SqrR. *Communicative & Integrative*

716 *Biology*. 10: e1329786.

717 Shimizu, T., and Masuda, S. (2020) Persulphide-responsive transcriptional regulation and
718 metabolism in bacteria. *The Journal of Biochemistry*. 167: 125–132.

719 Shimizu, T., Shen, J., Fang, M., Zhang, Y., Hori, K., Trinidad, J.C., et al. (2017) SqrR
720 functions as a master regulator of sulfide-dependent photosynthesis. *Proceedings of
721 the National Academy of Sciences of the United States of America*. 114: 2355–2360.

722 Smith, A.T., Pazicni, S., Marvin, K.A., Stevens, D.J., Paulsen, K.M., and Burstyn, J.N.
723 (2015) Functional Divergence of Heme-Thiolate Proteins: A Classification Based on
724 Spectroscopic Attributes. *Chemical Reviews*. 115: 2532–2558.

725 Sono, M., Dawsons, J.H., and Hager, L.P. (1984) The generation of a hyperporphyrin
726 spectrum upon thiol binding to ferric chloroperoxidase. *Journal of Biological
727 Chemistry*. 259: 13209–13216.

728 Sono, M., Sun, S., Modi, A., Hargrove, M.S., Molitor, B., Frankenberg-Dinkel, N., et al.
729 (2018) Spectroscopic evidence supporting neutral thiol ligation to ferrous heme iron.
730 *Journal of Biological Inorganic Chemistry*. 23: 1085–1092.

731 Sun, Y., Zeng, W., Benabbas, A., Ye, X., Denisov, I., Sligar, S.G., et al. (2013)
732 Investigations of heme ligation and ligand switching in cytochromes P450 and P420.
733 *Biochemistry*. 52: 5941–5951.

734 Vandeyara, M.A., Weiner, M.P., Hutton, C.J., and Batt, C.A. (1988) A simple and rapid
735 method for the selection of oligodeoxynucleotide-directed mutants. *Gene*. 65: 129–
736 133.

737 Wei, B., Zhang, W., Chao, J., Zhang, T., Zhao, T., Noctor, G., et al. (2017) Functional
738 analysis of the role of hydrogen sulfide in the regulation of dark-induced leaf
739 senescence in Arabidopsis. *Scientific Reports*. 7: 2615.

740 Yadav, P.K., Martinov, M., Vitvitsky, V., Seravalli, J., Wedmann, R., Filipovic, M.R., et al.
741 (2016) Biosynthesis and reactivity of cysteine persulfides in signaling. *Journal of the
742 American Chemical Society*. 138: 289–299.

743 Yang, J., Kim, K.D., Lucas, A., Drahos, K.E., Santos, C.S., Mury, S.P., et al. (2008) A
744 novel heme-regulatory motif mediates heme-dependent degradation of the circadian
745 factor period 2. *Molecular and cellular biology*. 28: 4697–4711.

746 Yi, L., and Ragsdale, S.W. (2007) Evidence that the heme regulatory motifs in heme
747 oxygenase-2 serve as a thiol/disulfide redox switch regulating heme binding. *Journal
748 of Biological Chemistry*. 282: 21056–21067.

749 Yin, L., Dragnea, V., and Bauer, C.E. (2012) PpsR, a regulator of heme and
750 bacteriochlorophyll biosynthesis, is a heme-sensing protein. *Journal of Biological*
751 *Chemistry*. 287: 13850–13858.
752

753 **Tables**

754

755 **Table 1**

756 Secondary structural composition of apo-SqrR, DTT reduced apo-SqrR, ferricyanide
 757 oxidized Heme-SqrR, dithionite reduced Heme-SqrR and dithionite and DTT reduced
 758 Heme-SqrR. Secondary structure contents (%) were estimated from the CD spectra shown
 759 in Fig. 2 using BeStSel program (Micsonai et al., 2015).

Sample	apo-SqrR			DTT reduced apo-SqrR			ferricyanide oxidized Heme-SqrR			dithionite reduced Heme-SqrR			Dithionite and DTT reduced Heme-SqrR		
	Helix (%)	Sheet (%)	Coil (%)	Helix (%)	Sheet (%)	Coil (%)	Helix (%)	Sheet (%)	Coil (%)	Helix (%)	Sheet (%)	Coil (%)	Helix (%)	Sheet (%)	Coil (%)
secondary structure contents	39.2	11.2	49.7	35.5	16.5	48.0	32.6	13.9	53.5	25.0	18.2	56.7	36.7	10.8	52.6

760

761 **Table 2**

762 Binding affinity of SqrR and Heme-SqrR untreated and fully DTT-reduced or treated with
 763 GSSH to *sqr* promoter DNA probes. ^{a-d} $P < 0.05$, *t*-test (compared pairwise). These data were
 764 obtained by analyses which were performed three times. Data shown are mean \pm S.E.

Protein	Conditions	EC ₅₀ (nM)
SqrR	reduced	40 (\pm 8) ^{a, c} , n=3
	GSSH-treated	79 (\pm 4) ^{a, d} , n=3
Heme-SqrR	reduced	211 (\pm 11) ^{b, c} , n=3
	GSSH-treated	240 (\pm 14) ^{b, d} , n=3

765

766 **Legends to Figures**

767

768 **Figure 1.** SqrR binds heme. **(A)** Sodium dodecyl sulfate-polyacrylamide gel electrophoresis
769 (SDS-PAGE) analysis of purified FLAG-tagged SqrR from *R. capsulatus*. An arrow indicates
770 the band of FLAG-tagged SqrR. The gel was stained by SYPRO Ruby protein gel stain
771 (Molecular Probes). **(B)** UV-visible spectrum of purified FLAG-tagged SqrR. **(C)** UV-visible
772 spectrum of hemin solution under oxidizing conditions (black line) and reducing conditions
773 (red line). Ferricyanide and dithionite was used for oxidizing and reducing conditions,
774 respectively. **(D)** UV-visible spectrum of Heme-SqrR under oxidizing conditions (black line),
775 dithionite reducing conditions (red line) and dithionite and DTT reducing conditions (blue
776 line). **(E)** Changes in UV-visible spectra of hemin upon sequential titration of SqrR into
777 hemin at pH 8.0. **(F)** Titration of SqrR into hemin. SqrR solution was titrated into a 10 μ M
778 hemin solution in incremental steps to a final ratio of 3.07:1. The change of Soret peaks at
779 375 nm indicates the formation of Heme-SqrR complex. **(G)** Binding constant of hemin-
780 SqrR interaction. Hemin was titrated into 1 μ M SqrR, with at least 5 min incubation time
781 between each step. The data were fitted with a one site binding model.

782

783 **Figure 2.** CD spectra of apo-SqrR (black line) and Heme-SqrR. apo-SqrR was reduced by
784 DTT (blue line). Heme-SqrR was oxidized by ferricyanide (green line) or reduced by
785 dithionite (red line). Dithionite reduced Heme-SqrR was also reduced by DTT (purple line).
786 The concentrations of protein were calculated using the Bradford method.

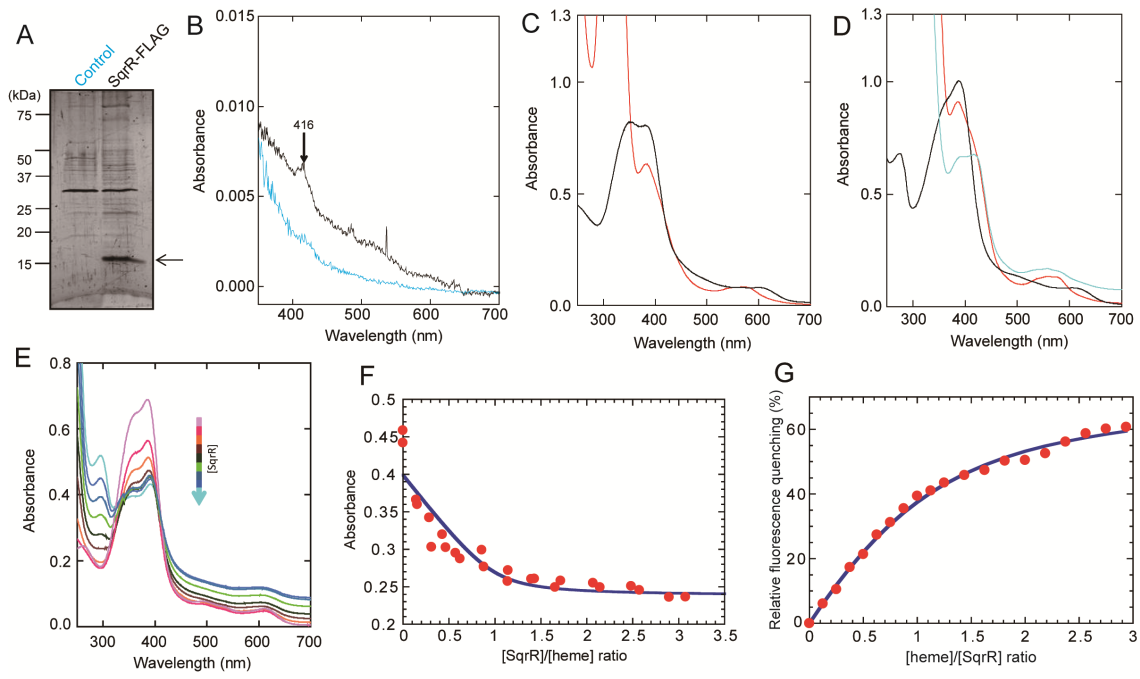
787

788 **Figure 3.** Binding affinity of DTT-reduced, Na₂S-treated, and (per)sulfide-treated
789 (Heme-)SqrR. **(A)** Gel mobility shift assay using a DNA probe of the *sqr* promoter region
790 under anaerobic conditions using from 24 nM to 60 nM DTT-reduced or Na₂S-treated SqrR.
791 **(B)** Gel mobility shift assay using a DNA probe of the *sqr* promoter region under anaerobic
792 conditions using from 60 nM to 240 nM DTT-reduced or Na₂S-treated Heme-SqrR. **(C)** Gel
793 mobility shift assay using a DNA probe of the *sqr* promoter region under anaerobic
794 conditions using DTT-reduced or GSSH-treated Heme-SqrR. This analysis was performed
795 three times, and similar results were obtained. **(D)** Binding isotherms of DTT-reduced (open
796 circles) and GSSH-treated (filled circles) Heme-SqrR. DNA-binding percentages were
797 generated by measuring the levels of shifted probes. Data shown are mean \pm S.E. (*error bars*).
798 **(E)** Binding isotherms of DTT-reduced (open circles) and GSSH-treated (filled circles) SqrR.

799 DNA-binding percentages were generated by measuring the levels of shifted probes. Data
800 shown are mean \pm S.E. (*error bars*).

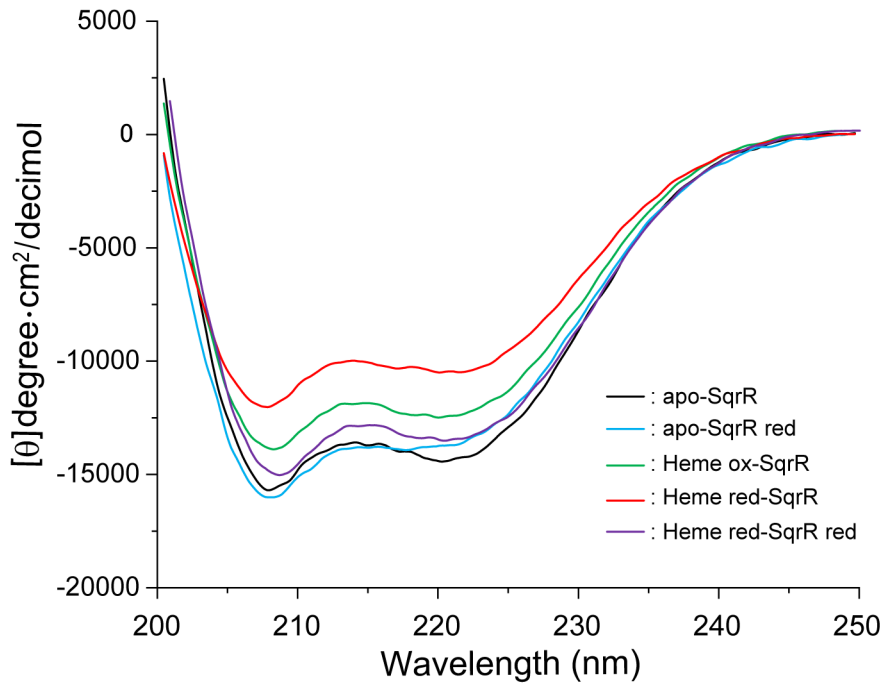
801

802 **Figure 4.** Heme content of cells and transcription of *sqr*. **(A)** Changes in intracellular heme
803 concentration after treatment with sulfide (filled circles) or without sulfide (open circles) in
804 WT. Data shown are mean \pm S.D. (*error bars*). **(B)** Change in relative level of transcripts of
805 *sqr* after treatment with sulfide (filled circles) or without sulfide (open circles) in WT. Data
806 shown are mean \pm S.E. (*error bars*). **(C)** Change in relative level of transcripts of *sqr* in the
807 absence of sulfide in *R. capsulatus* *sqrR*-FLAG strain (open square) and C41S *sqrR*-FLAG
808 mutant strain (filled square). Data shown are mean \pm S.E. (*error bars*). Asterisks indicate a
809 $P < 0.05$ significance using the Student's *t*-test between different data points from different
810 series at the same time point.



811

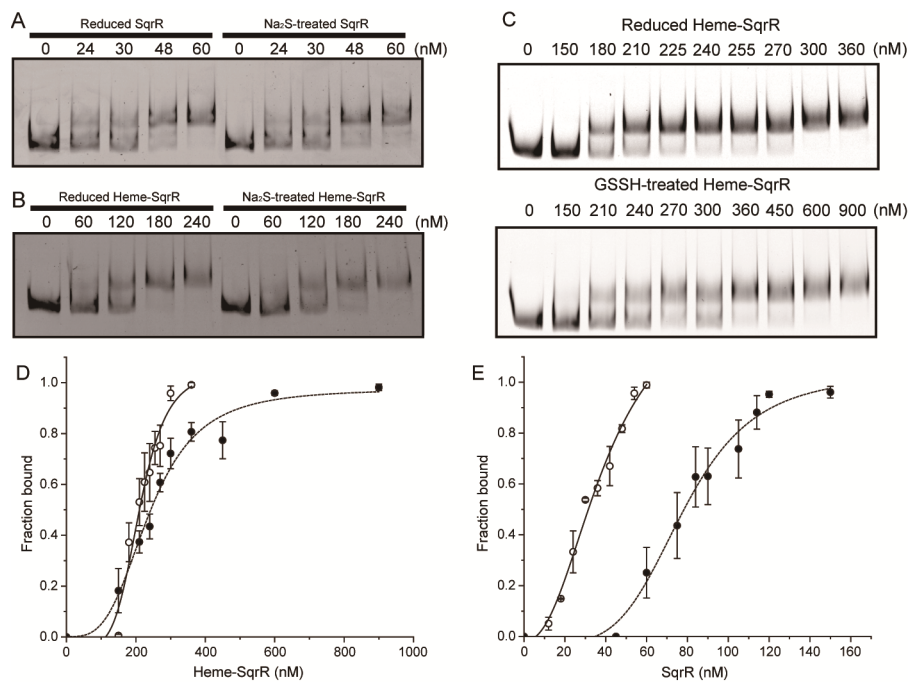
812 Figure 1



813

814 Figure 2

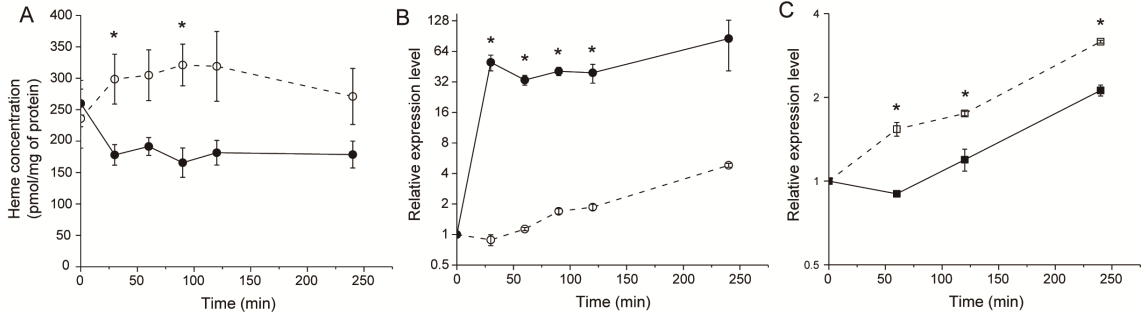
815



816

817

Figure 3



818

819 Figure 4

820 **Supplementary information**

821

822 **Repressor activity of SqrR, a master regulator of persulfide-responsive genes, is**
823 **regulated by heme coordination**

824

825 Takayuki Shimizu^{1, 2, 3} *, Yuuki Hayashi³, Munehito Arai^{3,4}, Shawn E. McGlynn², Tatsuru
826 Masuda³, Shinji Masuda^{1,2}

827

828 ¹Department of Life Science and Technology, Tokyo Institute of Technology, Kanagawa,
829 Japan

830 ²Earth-Life Science Institute, Tokyo Institute of Technology, Tokyo, Japan

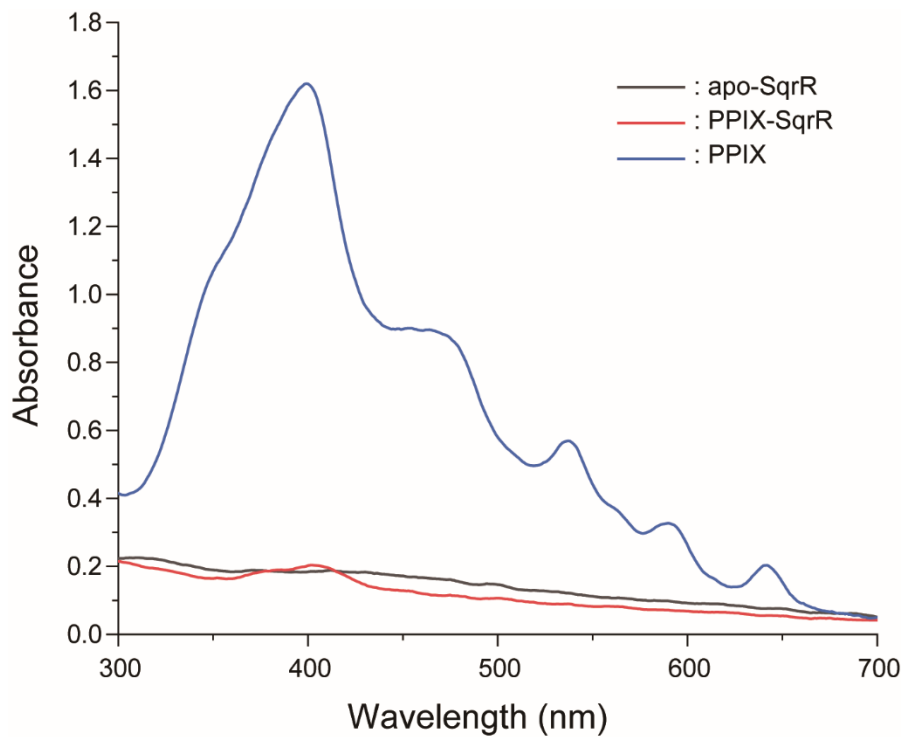
831 ³Graduate School of Arts and Sciences, The University of Tokyo, Tokyo, Japan

832 ⁴Department of Physics, The University of Tokyo, Tokyo, Japan

833

834 *Corresponding author: ctshimizu@g.ecc.u-tokyo.ac.jp

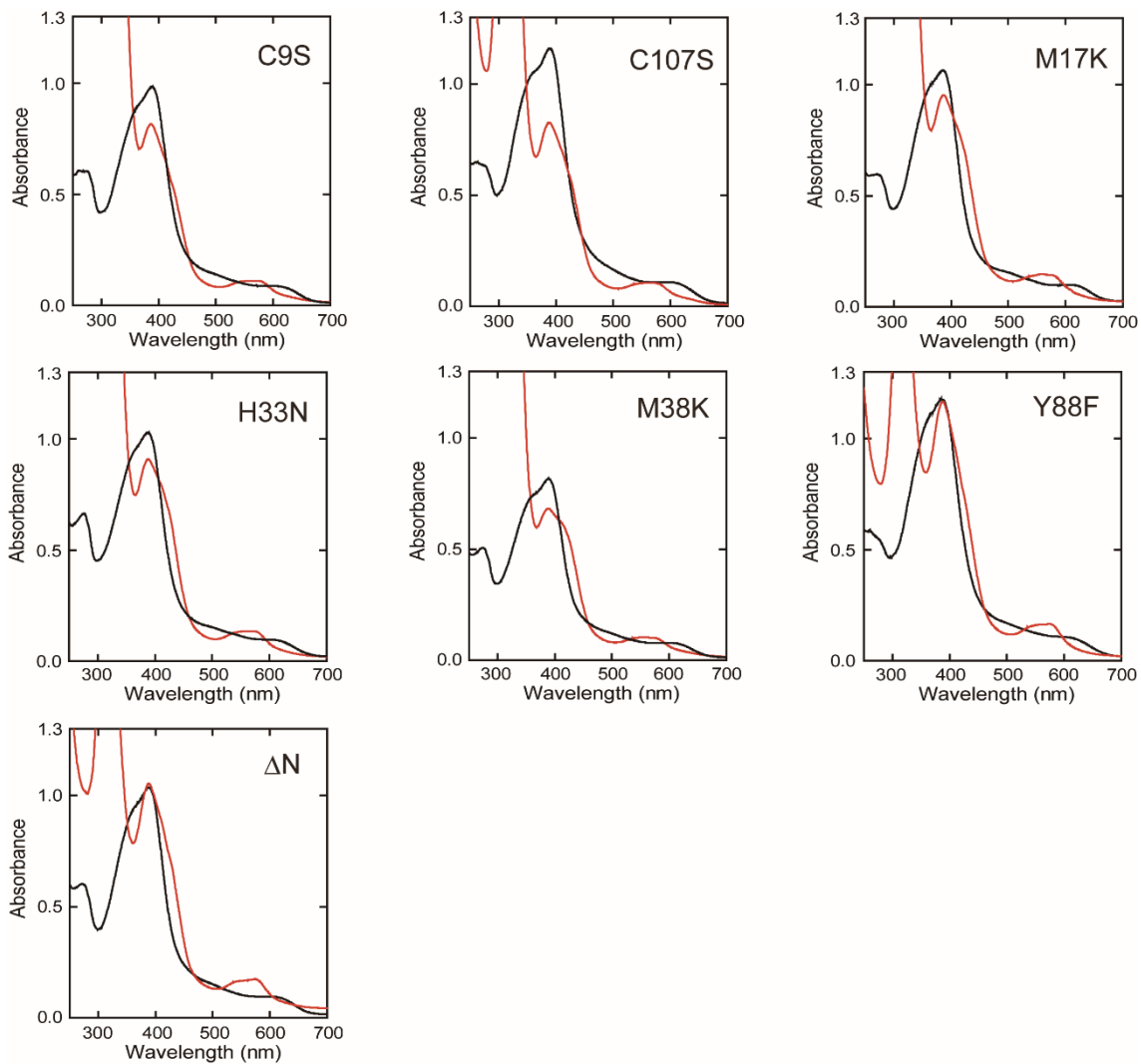
835



836

837 **Supplementary Figure 1.** UV-visible spectrum of Protoporphyrin IX (PPIX) solution (blue), apo-
838 SqrR (black) and PPIX-SqrR (red).

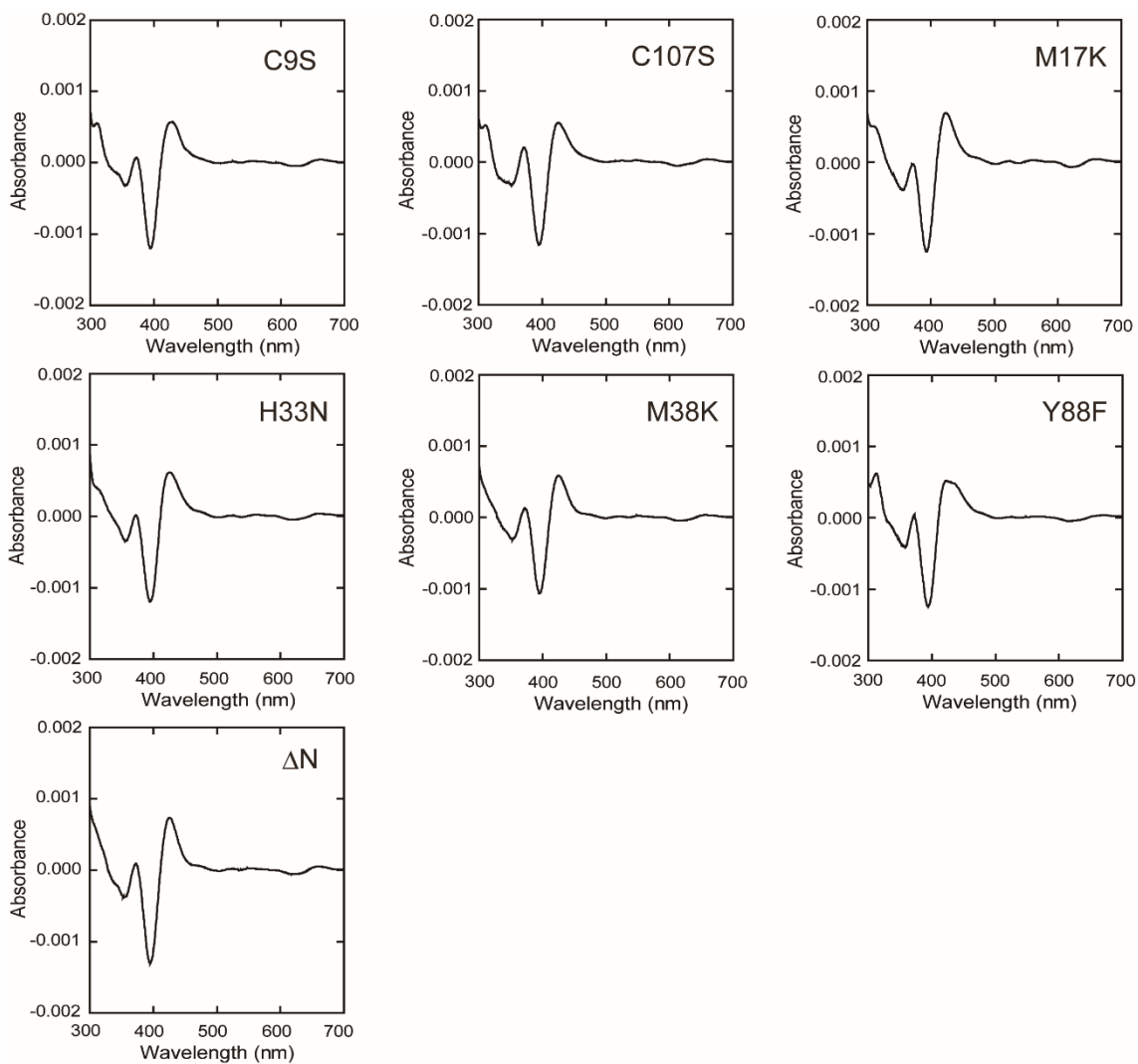
839



840

841 **Supplementary Figure 2.** UV-visible spectrum of each mutated SqrR. The spectra under oxidizing
 842 conditions (treated with ferricyanide) are shown with black line. The spectra under reducing
 843 conditions (treated with dithionite) are shown with red line. ΔN is SqrR lacking the N-terminal 15
 844 A.A.

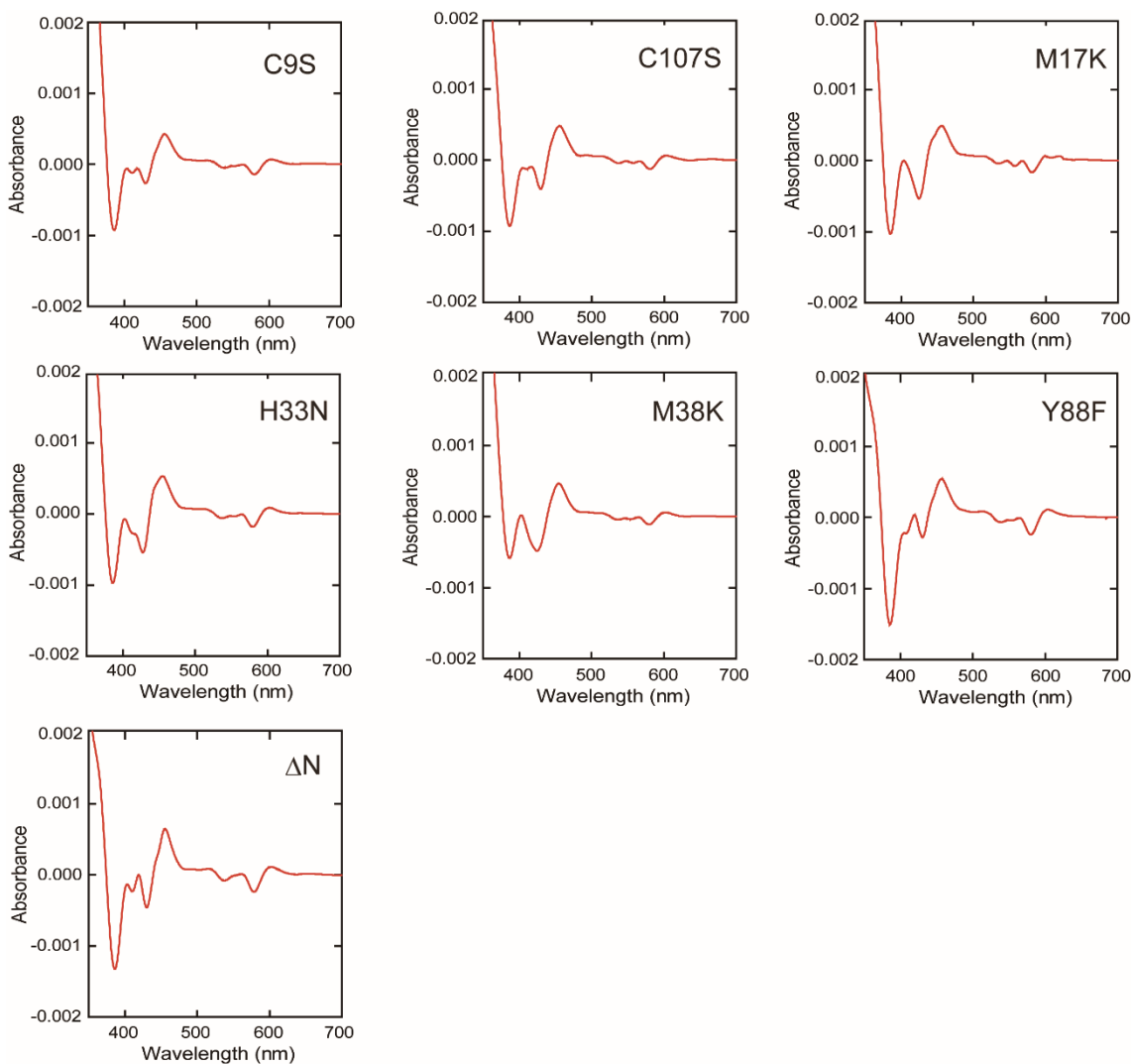
845



846

847 **Supplementary Figure 3.** Second-order derivative absorption spectra under oxidizing conditions of
 848 Supplementary figure 2. Double Soret peak is almost separated into ≈ 355 nm and ≈ 395 nm. All
 849 spectra show that ≈ 395 nm peak is dominant and it is similar to WT.

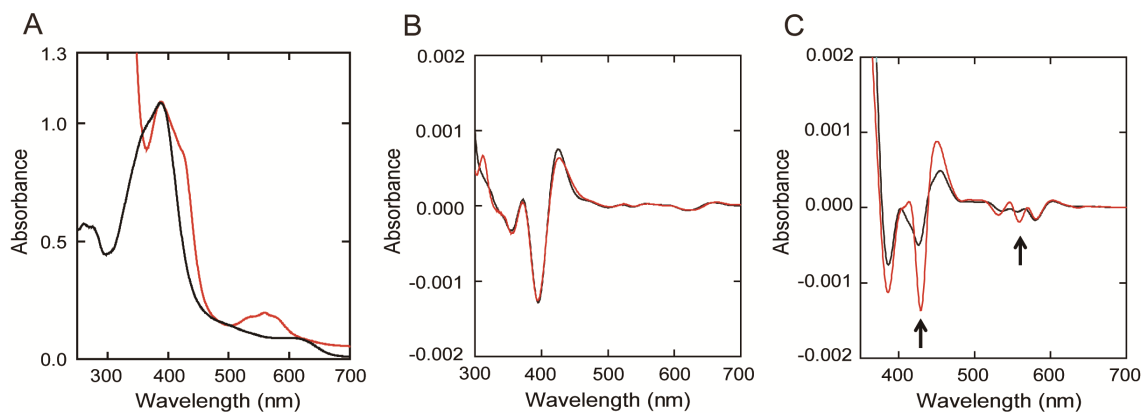
850



851

852 **Supplementary Figure 4.** Second-order derivative absorption spectra under the dithionite reducing
 853 conditions of Supplementary figure 2. The double Soret peak is almost separated into ≈ 387 nm and
 854 ≈ 427 nm and α and β peaks occur at 510-610 nm. All spectra show that the ≈ 387 nm peak is dominant
 855 and it is similar to WT. In the case of Y88F and ΔN (SqrR lacking the N-terminal 15 A.A.), the ≈ 387
 856 nm peak is much higher than ≈ 427 nm peak as compared with other SqrRs. It may be due to structural
 857 change by mutation because Tyr88 is located near a helix-turn-helix motif, and a Y88F mutant strain
 858 lacked repression activity by SqrR (data not shown).

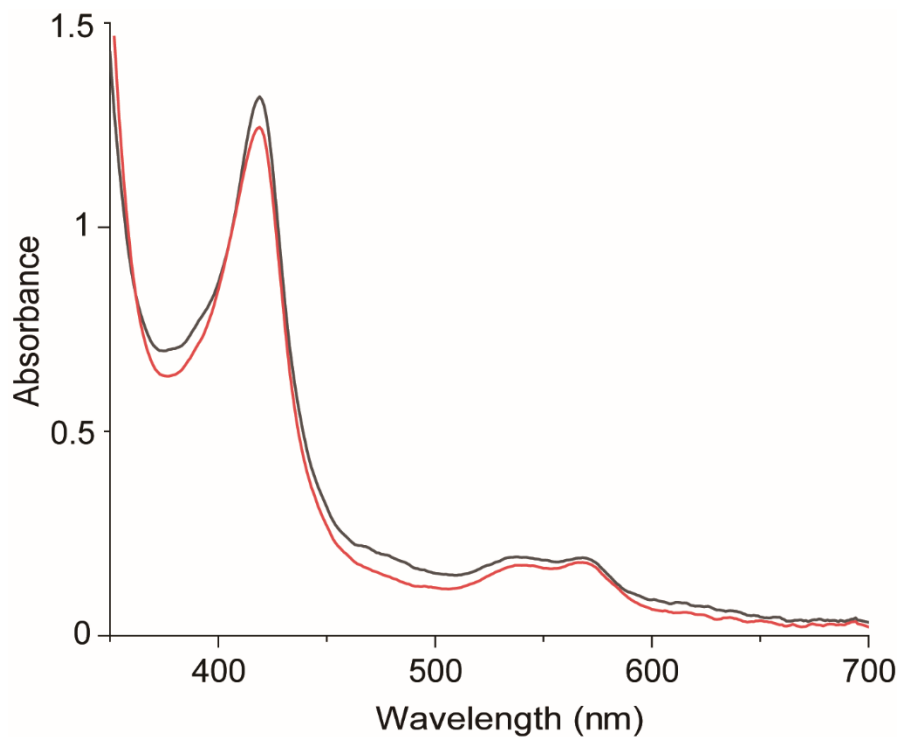
859



860

861 **Supplementary Figure 5.** Characterization of heme-coordination in SqrR. **(A)** UV-visible spectrum
 862 of C41S SqrR under ferricyanide oxidizing conditions (black line) and dithionite reducing
 863 conditions (red line) without DTT. **(B)** Second-order derivative absorption spectrum of WT (black
 864 line) and C41S SqrR (red line) under oxidizing conditions. **(C)** Second-order derivative absorption
 865 spectrum of WT (black line) and C41S SqrR (red line) under dithionite reducing conditions.

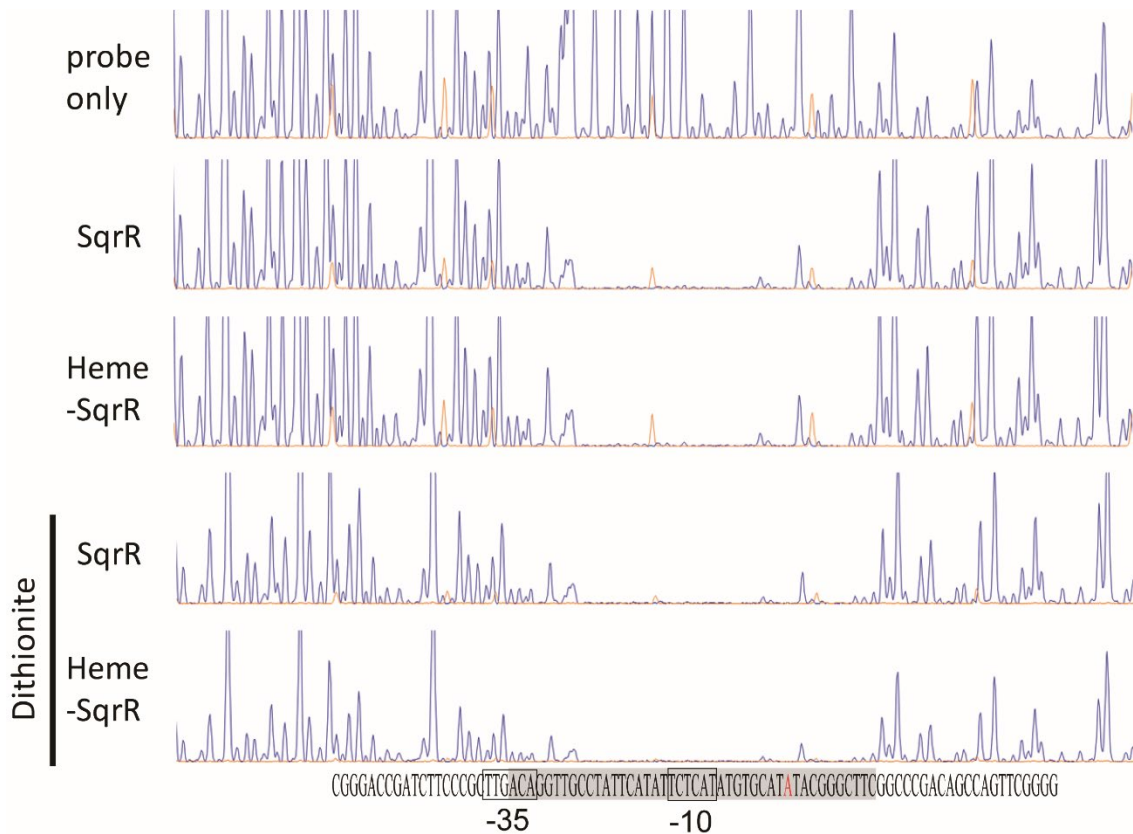
866



867

868 **Supplementary Figure 6.** UV-visible spectrum of dithionite- and DTT-reduced WT (black line) and
869 C41S (red line) Heme-SqrR treated with 100 μM CO releasing reagents CORM-3 at pH 7. 20 μM 0.5
870 mM DTT-reduced SqrR and 20 μM hemin were incubated for at least 20 minutes, then reduced with
871 a few grains of solid dithionite. After CORM-3 was mixed to solution, spectrum was recorded
872 immediately.

873



874

875 **Supplementary Figure 7.** DNase I footprint analysis of SqrR and Heme-SqrR to the *sqr* promoter
 876 region. Blue and orange peaks are the DNase I non-protection regions and the 500 LIZ™ Size
 877 Standard (Applied Biosystems), respectively. Regions corresponding to the DNase I protection
 878 regions are shown in gray background. The -35 and -10 σ -subunit recognition sequences are boxed
 879 letter on the bottom of figure, with the transcription start site shaded red.

880



881

882 **Supplementary Figure 8.** Detection of standard heme in the absence and presence of final 0.6 mM
883 sodium sulfide. The numbers on the picture show the heme concentration.

884